Since January 2020 Elsevier has created a COVID-19 resource centre with free information in English and Mandarin on the novel coronavirus COVID-19. The COVID-19 resource centre is hosted on Elsevier Connect, the company's public news and information website.

Journal of Molecular Structure 1247 (2022) 131348

Contents lists available at ScienceDirect

Journal of Molecular Structure

journal homepage: www.elsevier.com/locate/molstr

[Cu(dipicolinoylamide)(NO_3)(H_2O)] as anti-COVID-19 and antibacterial drug candidate: Design, synthesis, crystal structure, DFT and molecular docking

Laila H. Abdel-Rahman[a], Maram T. Basha[b], Badriah Saad Al-Farhan[c], Mohamed R. Shehata[d], Shaaban K. Mohamed[e,f,*], Youssef Ramli[g,*]

[a] Chemistry Department, Faculty of Science, Sohag University, 82524 Sohag, Egypt
[b] University of Jeddah, College of Science, Department of Chemistry, Jeddah, Saudi Arabia
[c] Chemistry Department, Faculty of Girls for Science, King Khalid University, Abha, Saudi Arabia
[d] Chemistry Department, Faculty of Science, Cairo University, Giza, Egypt
[e] Chemistry and Environmental Division, Manchester Metropolitan University, Manchester M1 6GD, England
[f] Chemistry Department, Faculty of Science, Minia University, 61519 El-Minia, Egypt
[g] Laboratory of Medicinal Chemistry, Drug Sciences Research Center, Faculty of Medicine and Pharmacy, Mohammed V University in Rabat, Morocco

ARTICLE INFO

Article history:
Received 20 April 2021
Revised 12 August 2021
Accepted 19 August 2021
Available online 22 August 2021

Keywords:
Copper (II)
2,4,6-ris(2-pyridyl)-,3,5-triazine
N-picolinoylpicolinamide, crystal structure
COVID-19, antimicrobial, DFT, docking

ABSTRACT

For first time the new N-picolinoypicolinlamide was obtained as in situ ligand during the reaction of 2,4,6-ris(2-pyridyl)-,3,5-triazine with aqueous solution of $CuNO_3{\cdot}3H_2O$ and formed the corresponding complex [Cu(dipicolinoylamide)(NO_3)(H_2O)]. The crystal structure of the obtained complex was determined by x-ray structure. The complex crystallizes in space group $P2_1/n$, a = 10.2782(9) Å, b = 7.5173(6) Å, c = 17.738(2) Å, α = 90.00°, β = 91.368(1)°, γ = 90.00°, V = 1370.1(2) Å3, Z = 4. The copper center has a distorted octahedral geometry. DFT calculations show good agreement between theoretical and X-ray data. The Molecular docking studies were executed to consider the nature of binding and binding affinity of the synthesized compounds with the receptor of COVID-19 main protease viral protein (PDB ID: 6lu7), the receptor of gram –ve bacteria (Escherichia coli, PDB ID: 1fj4) and the receptor of gram +ve bacteria (Staphylococcus aureus, PDB ID: 3q8u and Proteus PDB ID: 5i39) and with human DNA. Finally, in silico ADMET predictions was also examined.

1. Introduction

As of 03 March 2021, there have been 115.128.349 confirmed cases of coronavirus disease 2019(COVID-19), Severe Acute Respiratory Syndrome coronavirus 2 (SARS-CoV-2) infection that causes the current global health crisis, including 2.558.059 deaths in 216 countries or territories, reported to the World Health Organization (WHO). Since the emergence of COVID-19, in December 2019 in Wuhan, scientists all over the world are working in a race to develop vaccines for prevention and new drugs for treatment of the disease.

Previous reports suggested a beneficial effect of traditional medicine (TM)/herbal medicines (HMs), in COVID-19 [1-3]. Similarly, proposed agents to treat COVID-19 include hydroxychloroquine [4], glucocorticoids [5], baricitinib [6], anakinra [7,8], and direct antivirals [9]. Currently, several molecules are being tested for their efficacy on COVID-19, some of which have reached clinical trials, while others are still in preclinical phase [10-14]. In this case, remdesivir is the first and only drug approved by the U.S. Food and Drug Administration (FDA) for COVID-19 in the USA [15].

The SARS-CoV-2 main protease plays an important role in viral replication. In fact, it is a key target for COVID-19 drug discovery. Other important roles in understanding the molecular mechanism in drug discovery are the binding affinity and structure of protein–drug complexes. Since COVID-19 is not a rare disease, the development of other more scalable treatments is still of great importance. Notably, a new candidate to inhibit binding between the COVID-19 main protease and the angiotensin converting enzyme-2, on the cell surface. In view of these facts, we have been stimulated to screen, in silico, the interaction between the main protease active site with the complex in the title. Finally, in silico antibacterial activities predictions were also examined.

In their work with these compounds, Lerner and Lippard [16,17] found that ptz undergoes hydrolytic reaction in the presence of

* Corresponding authors.
E-mail addresses: shaabankamel@yahoo.com (S.K. Mohamed), y.ramli@um5s.net.ma (Y. Ramli).

https://doi.org/10.1016/j.molstruc.2021.131348
0022-2860/

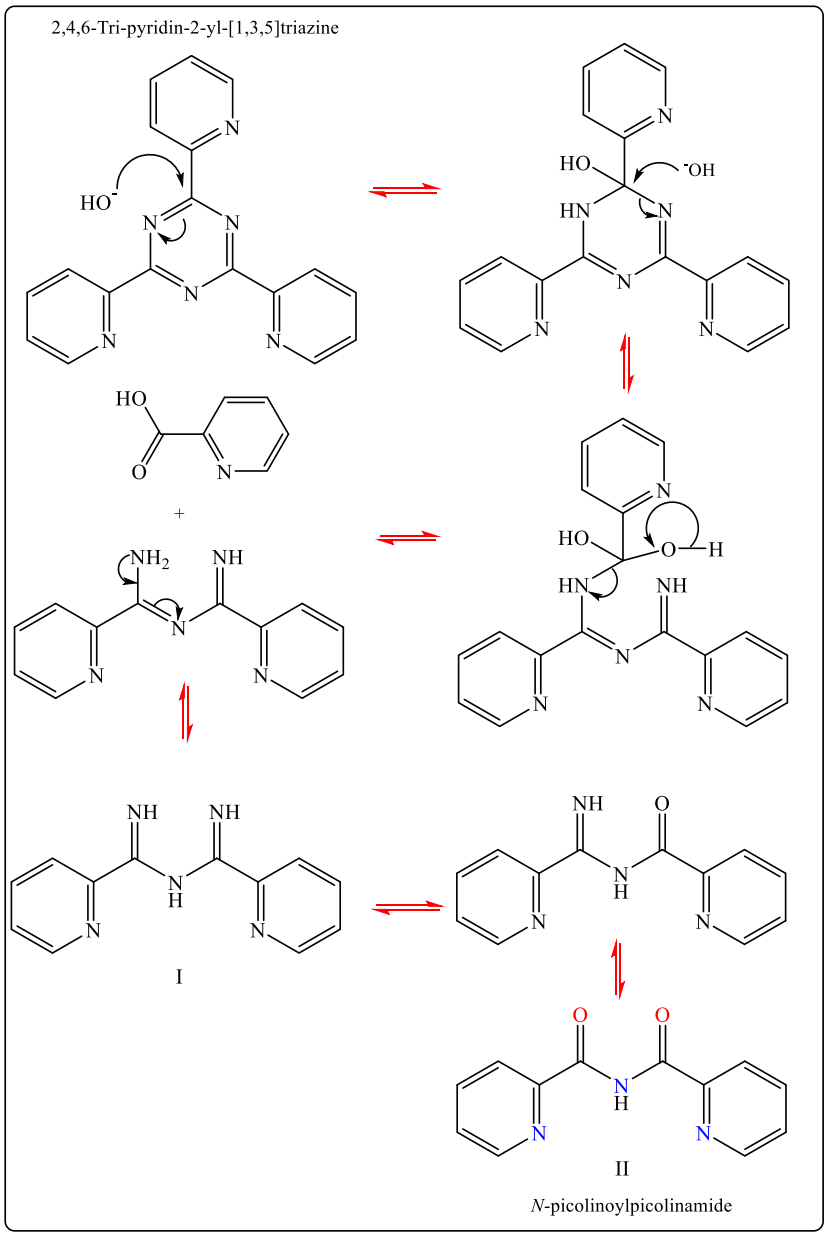

Scheme 1. Mechanism of hydrolysis of 2,4,6-tri(pyridin-2-yl)−1,3,5-triazine (ptz).

Cu(II) in aqueous media. They also reported a crystal structure of copper (II) complex with a hydrolytic product of ptz. On the basis of the Cu-N bond distances and angles of the carbonyl carbon atoms within the chelate ring, it was suggested that the coordination of ptz induces an angular strain, thus permitting a nucleophilic attack at the carbon atoms of the triazine ring by the solvent, which in turn results in the hydrolysis of ptz [17,19]. The hydrolysis process of ptz (Scheme 1) involves the formation of several intermediates, namely two imino nitrogen $(ptzN_2)^-$ groups, one imino and one carbonyl ($ptNO^-$) group each, and finally two carbonyl groups (Hdpa) [18,19].

We also describe the synthesis of a the complex [Cu(dipicolinoylamide)$(NO_3)(H_2O)$], (Scheme 2), and report the single-crystal X-ray structure, DFT molecular optimization and from molecular docking studies, the likely binding of this complex in the actives sites. Moreover, the molecular docking studies have been performed to understand the nature of binding of the ligand and the Cu(II) complex with human DNA. Finally, in silico ADMET predictions was carried to study the toxic effects, absorption and solubility characteristics.

2. Experimental

2.1. Materials

All chemicals were of the highest pure commercially available. All solvents were purified by distillation according to standard methods.

2.2. Synthesis of the complex [Cu(dpa)$(NO_3)(H_2O)$]

Ten milliliters of an aqueous solution of $CuNO_3{\cdot}3H_2O$ (0.24 g, 1 mmol) were added to 40 ml of (0.312 g, 1 mmol) of 2,4,6-tri(pyridin-2-yl)−1,3,5-triazine (ptz) and 2 ml of a methanolic solution of KOH 2 N to adjust the pH of the mixture to 8–9. A blue solution was formed immediatly (see Schemes 1 and 2). Slow evap-

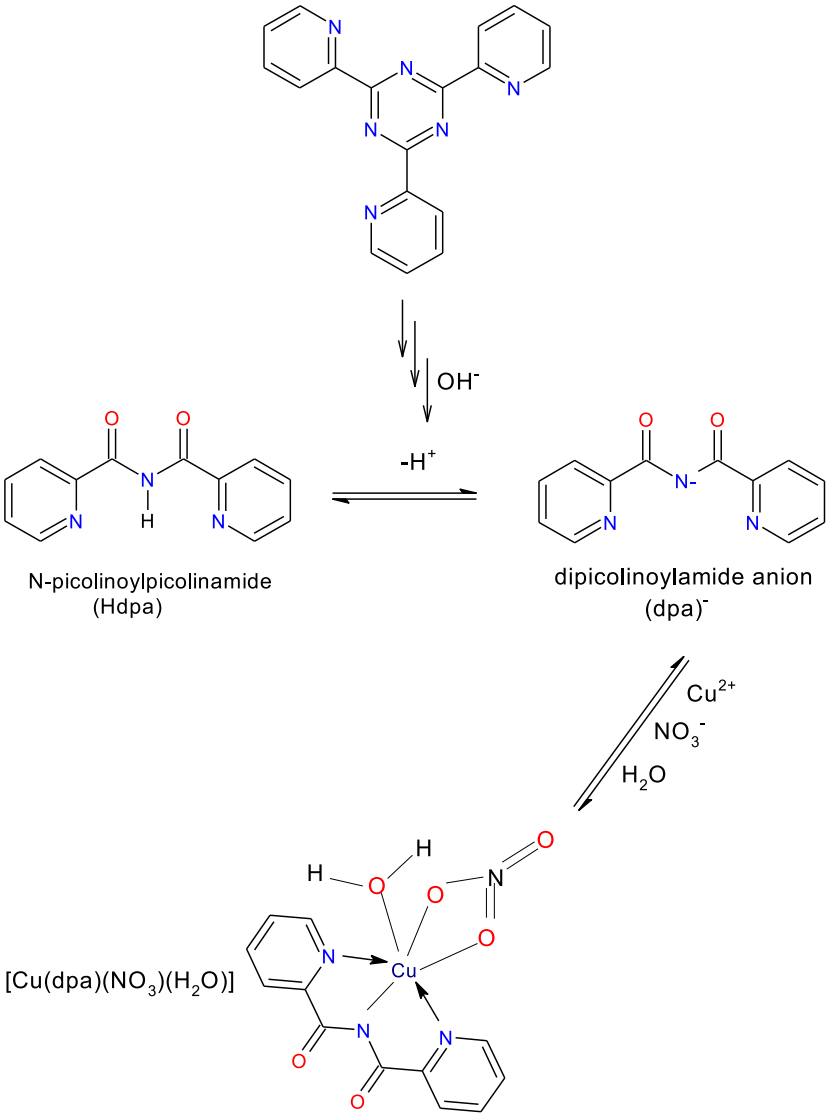

Scheme 2. Mechanism of formation of [Cu(dpa)(NO_3)(H_2O)] complex.

oration of the solution yielded blue crystals, yield 57%. Analytical data for $C_{12}H_{10}CuN_4O_6$: Anal. Found C, 38.90; H, 2.68; N, 15.08. Calc.: C, 38.98; H, 2.73; N, 15.15.

2.3. X-ray data collection and structure refinement

Crystals of the complex were mountaineer on glass fibers. Diffraction data were recorded on a Burker-AXS Smart Apex system equipped with a graphite monochromatic Mo Kα radiation (λ=0.71073 Å). The data were collected using SMART, and the integration was performed using SAINT [20]. An empirical absorption correction was carried out using SADABS [21]. The structure was solved with direct methods and refined by full matrix least square methods based on F^2, using the structure determination and graphics package SHELXTL [22] based on SHELX 97 [23,24]. Hydrogen atoms were included at calculated positions using a riding model.

2.4. DFT molecular optimization

The lowest energy configurations had been calculated, applying DFT/B3LYP/ GENCEP level theory with the Gaussian09 program [25]. LANL2DZ basis set for copper atom and 6–311 g++(d,p) basis set for C, N, O and H [26].

2.5. Molecular docking

Molecular docking studies were performed using MOA2015 software [27], in order to find out the possible binding modes of the ligand and the complex against certain protein. The Molecular docking studies were executed to consider the nature of binding and binding affinity of the synthesized compounds with the receptor of COVID-19 main protease viral protein (PDB ID: 6lu7), [28] gram –ve bacteria (Escherichia coli, PDB ID: 1fj4) [29] and the receptor of gram +ve bacteria (Staphylococcus aureus, PDB ID: 3q8u [30] and Proteus PDB ID: 5i39) [31]. The structure of ligand and complex were created in PDB file format from the output of Gaussian09 software. The crystal structures of the receptors were downloaded from the protein data bank (http://www.rcsb.org./pdb).

2.6. ADMET prediction

Absorption, Distribution, Metabolism and Toxicity (ADMET) studies. The molecular structure of the ligand was submitted to

ADMETlab 2.0 server (https://admetmesh.scbdd.com/) to examine their different pharmacokinetic and pharmacodynamic parameters including blood-brain barrier penetration, human intestinal absorption, Caco-2 permeability, cytochrome P450 inhibition, solubility, cytochrome P (CYP) inhibitory promiscuity, carcioge city, rat oral acute toxicity, skin sensitization and respiratory toxicity.

3. Results and discussion

3.1. The chemistry and crystal structure determination of [Cu(dpa)(NO_3)(H_2O)]

The reaction of 2,4,6-Tris(2-pyridyl)−1,3,5-triazine (ptz) and copper(II) nitrate in methanol-water resulted in the hydrolysis of ptz, giving rise to dipicolinoylamide anion $(dpa)^-$ and offering the complex [Cu(dpa)(NO_3)(H_2O)]. The reaction mechanism was assumed to proceed via a nucleophile attack of the 2 OH groups of base at the one double bond of triazine ring followed by elimination pyridine-2-carboxylic acid to afford N-(iminopyridin-3-yl-methyl)pyridine-2-carboxamidine (I), which was easily oxidized to the corresponding Pyridine-2-carboxylic acid(pyridine-2-carbonyl)-amide (II) in absence of metal ions. The later compound is stabilized by capture of metal ions to afford the corresponding complexes (Scheme 2).

The copper (II) ion shows a distorted octahedral structure. The coordination sphere around Cu(II) is very distorted, most likely as a result of the bidentate binding mode of the nitrate ion. The equatorial plane is formed by three nitrogen atoms from the ligand and the oxygen atom O(3) from a bidentate nitrate anion, with dihedral angle of about 7.510° The axial positions are occupied by the oxygen atom O(6) from a water molecule and by the other oxygen atom O(4) of the bidentate nitrate anion.

The Cu-N bond distances are in the range 1.932(1)−1.999(1) Å and the equatorial plane cis-angles around the Cu(II) ion vary from 82.01(6) ° to 94.07(6) ° (Table 2). These values are similar to those found in other previously reported copper(II) complexes with dpa^- [23]. The axial bond distance Cu-O4 (2.788(1) Å) is significantly longer than the equatorial one Cu-O3 (1.963(1) Å) and the axial bond angle O(4)-Cu(1)-O(6) is 132.27(5)°. These data are typical for the strained bidentate binding mode of nitrate which is at the origin of the distortion from the ideal octahedral geometry [32-34].

The crystallographic data are given in Table 1. Selected bond length and angles are given in Table 2. Complete bond length and bond angles, anisotropic thermal parameters and calculated hydrogen coordinates are deposited as supplementary materials. The drawings of the molecular structure with the atomic labeling schemes are given in Fig. 1 for the compound [Cu(dpa)(NO_3)(H_2O)].

Table 1
Crystallographic Data for Aqua-(nitrato-O, O')-(bis(2-pyridylcarbonyl) amido-N, N', N")-copper (II).

Formula	C_{12} H_{10} Cu N_4 O_6	F(000)	748
F. w.	369.78	Θ range	2.3–28.3°
Crystal system	Monoclinic	Index ranges	$-13 \le h \le 13$
Space group	$P2_1/n$		$-9 \le k \le 10$
a (Å)	10.2782(9)		$-22 \le l \le 22$
b (Å)	7.5173(6)	N collect	11,520
c (Å)	17.738(2)	N indep	3273
β (°)	91.368(1)	N obs	2994 reflections
V (Å^3)	1370.1(2)		with $I \ge 2\sigma(I)$
Z	4	$(\Delta/\sigma)_{max}$	0.001
T (K)	295	S	1.06
λ (Å)	0.71073	wR(F2)	0.075
$D_{x\ calc}$ (g.cm^{-3})	1.793	$\Delta\rho_{max}$	0.30 e Å^{-3}
μ (mm^{-1})	1.634	$\Delta\rho_{min}$	−0.32 e Å^{-3}

3.2. Molecular DFT calculation

3.2.1. Ligand (Hdpa)

Fig. 2 shows the optimized structure of the ligand as the lowest energy configurations. Almost all atoms are in one plane due to sp^2 hybridization of all carbon atoms. The natural charges obtained from Natural Bond Orbital Analysis (NBO) show that the active sites for Hdpa are O1(−0.550), O2(−0.550), N1(−0.467), N3(−0.467), N2(−0.666) and H9(+0.452). So, the metal ions prefer tridentate coordination to N1, N2 and N3, after the ionization of $(H9)^+$ forming two stable 5-membered rings.

3.2.2. [Cu(dpa)(NO_3)(H_2O)]

The optimized structure of the complex [Cu(dpa)(NO_3)(H_2O)] as the lowest energy configuration is shown in Figs. 3. The copper atom is six-coordinate in a very distorted octahedral geometry with water O6 and O4 of nitrate in axial position and atoms N1, N2, N3 and O3 are almost in one plane deviated by −1.846°, Table 2. All atoms of the ligand, copper atom and O3 of nitrate are almost in one plane.

The distances between N1 - - - N2, N2 - - - N3 and N1 - - - N3 are decreased from 2.677, 2.677 and 4.123 Å in the ligand to 2.629, 2.629 and 4.010 Å in the complex, respectively.

Table 2
Comparing the important x-ray and DFT optimized bond lengths (Å) and bond angles (°) of [Cu(dpa)(NO_3)(H_2O)].

Type of bond	Bond length (Å) X-Ray	DFT	Type of Angle	Angle (°) X-Ray	DFT
Cu-N1	1.993(2)	2.024	N1-Cu-N2	82.71(6)	82.21
Cu-N2	1.932(1)	1.975	N2-Cu-N3	82.01(6)	82.06
Cu-N3	1.999(1)	2.029	N1-Cu-O3	101.17(6)	98.79
Cu-O3	1.963(1)	2.020	N3-Cu-O3	94.07(6)	96.46
Cu-O4	2.787(2)	2.874	O6-Cu-N1	89.50(6)	93.55
Cu-O6	2.375(1)	2.325	O6-Cu-N2	96.56(5)	112.6
N2-C6	1.358(2)	1.378	O6-Cu-N3	102.28(6)	97.83
N2-C7	1.360(2)	1.376	O6-Cu-O3	84.15(5)	71.65
N1-C5	1.345(2)	1.357	O4-Cu-N1	86.25(5)	90.75
N3-C8	1.340(2)	1.358	O4-Cu-N2	129.76(5)	124.6
			O4-Cu-N3	95.79(5)	93.42
C5-C6	1.516(2)	1.507	O4-Cu-O3	50.50(5)	51.18
C7-C8	1.514(2)	1.509	O4-Cu-O6	132.27(5)	122.6
N1 - - - N2	2.593	2.629	N1-Cu-N3	161.65(6)	163.2
N2 - - - N3	2.579	2.629	N2-Cu-O3	176.07(6)	175.6
N1 - - - N3	3.940	4.010	N1-N2-N3-O3	7.510*	1.693*

*dihedral angle.

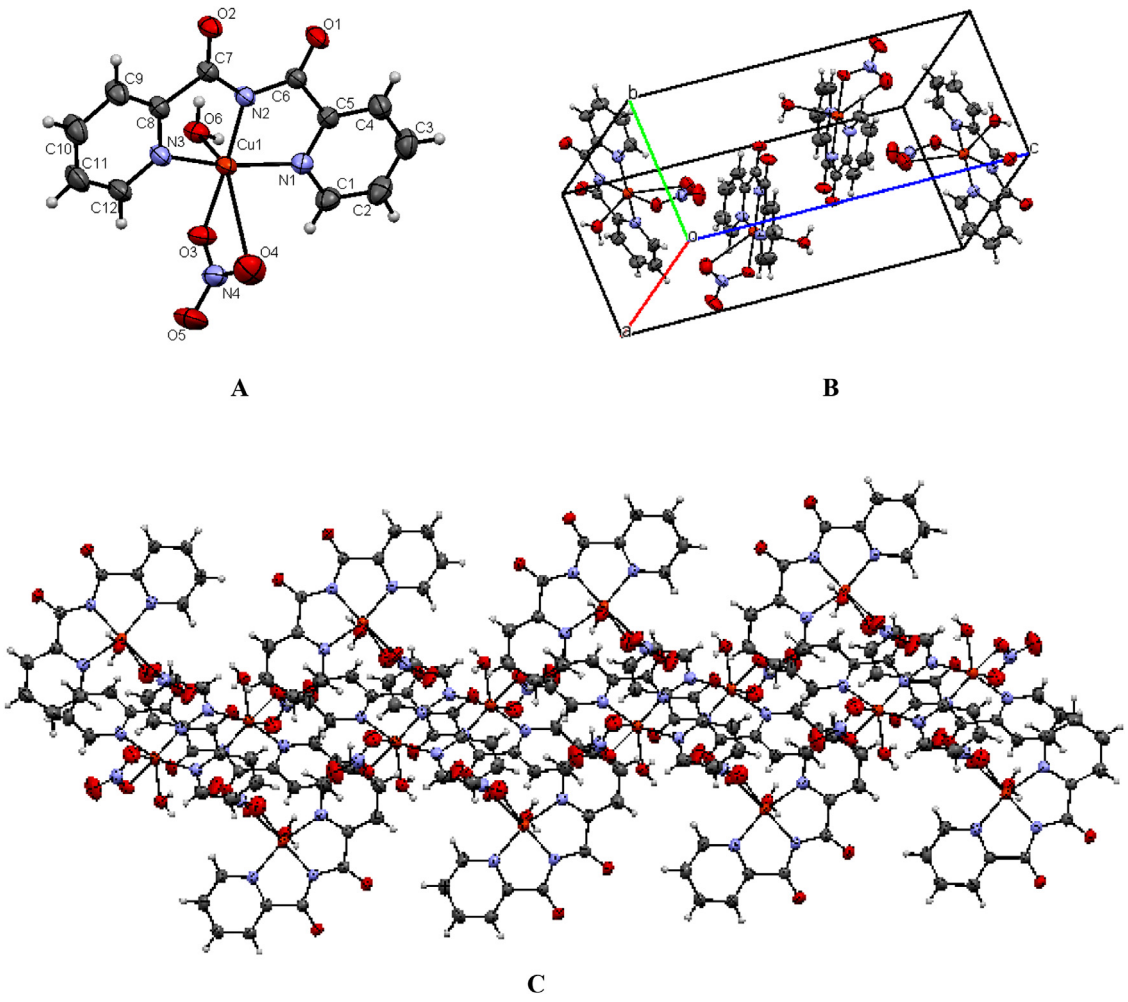

Fig. 1. (A) ORTEP drawing of (30% probability level) of [Cu(dpa)(NO_3)(H_2O)]. (B) Unit cell of [Cu(dpa)(NO_3)(H_2O)] crystal with four molecules per unit cell. (C) Close pac.

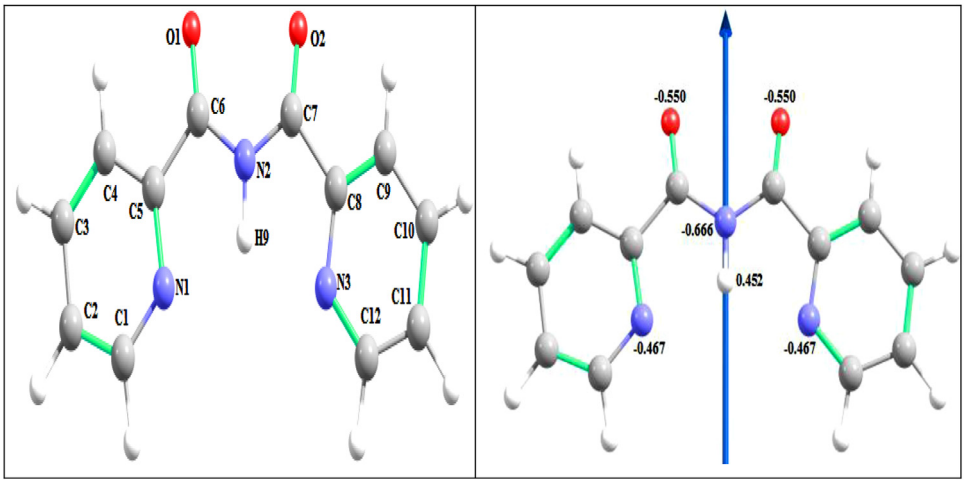

Fig. 2. The optimized structure of ligand.

The natural charges computed from the NBO-analysis on the coordinated atoms in [Cu(dpa)(NO_3)(H_2O)] are: Cu (+0.977), N1(−0.487), N2(−0.700), N3(−0.495), O3(−0.622), O4(−0.412) and O6(−0.890). The natural charge on O4 is −0.412, which is less than those for O3 and O6. This agrees with the larger distance between Cu atom and O4, 2.874 Å (2.787 Å x-ray) than distances between Cu-O3, 2.020 Å (1.963 Å x-ray), and Cu-O6, 2.325 Å (2.375 Å x-ray).

Fig. 4, shows the MEP surface is to locate the positive (blue color) and negative (red color, it is bound loosely or excess electrons) charged electrostatic potential in the molecule. The computed total energy, the highest occupied molecular orbital (HOMO)

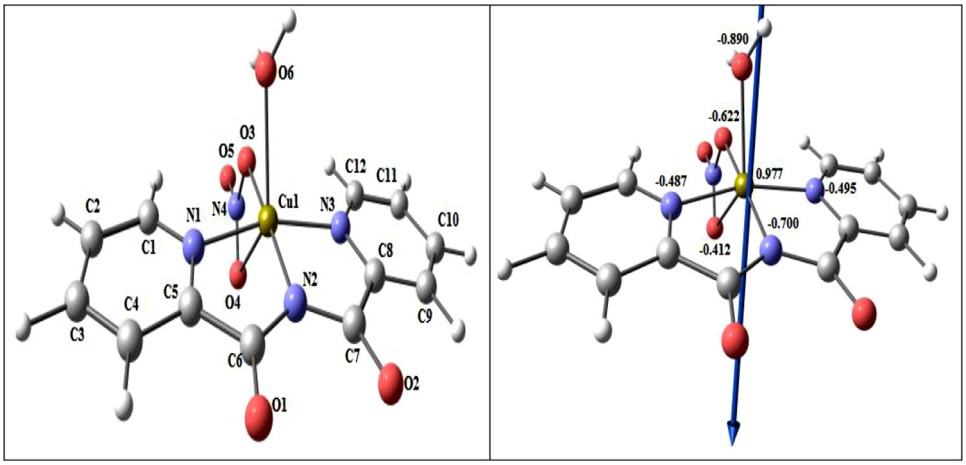

Fig. 3. The optimized structure, the vector of the dipole moment, and the natural charges on active centers of [Cu(dpa)(NO_3)(H_2O)].

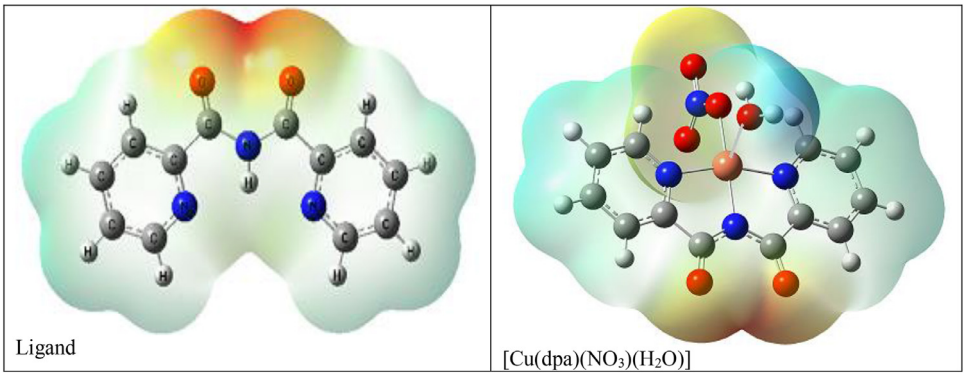

Fig. 4. Molecular electrostatic potential (MEP) surface of ligand and [Cu(dpa)(NO_3) (H_2O)] complex .

Table 3
Calculated energies of ligand and [Cu(dpa)(NO_3)(H_2O)] complex.

	E[a]	HOMO[b]	LUMO[c]	E_g[d]	Dipole moment[e]
Ligand	−777.637	−6.9741	−2.3043	4.6698	5.6564
Complex	−1329.724	−6.8296	−3.1130	3.7166	5.8778

[a] E: the total energy (a.u.). [b]HOMO: highest occupied molecular orbital (eV).
[c] LUMO: lowest unoccupied molecular orbital (eV).
[d] E_g=E_{LUMO}- E_{HOMO} (eV). [e]dipole moment (Debye).

energies, the lowest unoccupied molecular orbital (LUMO) energies and the dipole moment for the ligands and complexes were calculated, Table 3. The more negative values of total energy of the complex than that of the free ligand indicates that the complex is more stable than the free ligand and the energy gap (E_g) = E_{LUMO} - E_{HOMO} are smaller in case of complex than that of ligand due to chelation of ligand to metal ions, Table 3. The lowering of E_g in complexes compared to that of ligand explains the charge transfer interactions upon complex formation, Fig. 5.

3.3. Molecular docking

3.3.1. Docking on COVID-19 main protease viral protein (PDB ID: 6lu7)

In the present study, the binding free energy of the ligand and the metal complex with the active sites of the receptor of COVID-19 main protease viral protein (PDB ID: 6lu7), organism (Severe acute respiratory syndrome coronavirus 2) are found to be −5.6 and −20.2 kcal/mol for the ligand and the Cu(II) complex; respectively, Table 4. The more negative the binding energy the stronger interaction. So, the interaction are in the order of Cu(II) complex > L.

The 2D and 3D plot of the interaction between L and Cu(II) complex with the active site of the receptor of viral protein (PDB ID: 6lu7) are shown in Figs. 6 and 7.

3.3.2. Docking on gram +ve bacteria: proteus vulgaris (PDB ID: 6lu7)

In the present study, the binding free energy of the ligand and the metal complex with the active sites of the receptor of gram +ve bacteria: Proteus vulgaris (PDB ID: 5i39) are found to be −7.6 and −30.2 kcal/mol for the ligand and the Cu(II) complex; respectively, Table 5. The more negative the binding energy the stronger interaction. So, the interaction are in the order of Cu(II) complex > L.

The 2D and 3D plot of the interaction between L and Cu(II) complex with the active site of the receptor of Proteus vulgaris (gram +ve bacteria) (PDB ID: 5i39) are shown in Figs. 8 and 9.

3.3.3. Docking on gram -ve bacteria:E. coli (PDB ID: 1fj4)

In the present study, the binding free energy of the ligand and the metal complex with the active sites of the receptor of gram -

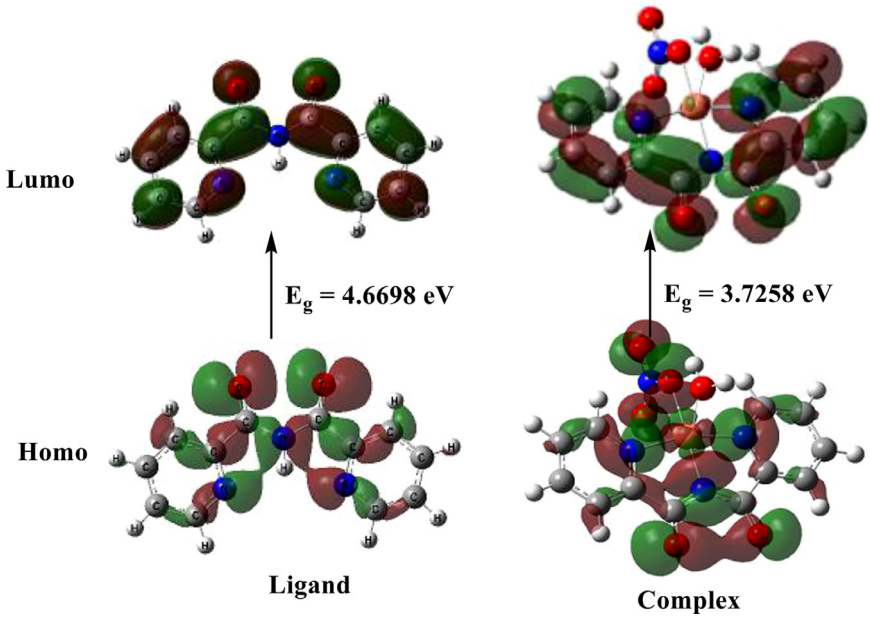

Fig. 5. HOMO and LUMO charge density maps of ligand and [Cu(dpa)(NO_3)(H_2O)] complex.

Table 4
The Docking interaction data calculations of ligand and Cu(II) complex with the active sites of the receptor of COVID-19 main protease viral protein (PDB ID: 6lu7).

	Receptor	Interaction	Distance(Å)*	E (kcal/mol)
L				
N 14	SD MET 165	H-donor	3.24 (2.34)	−4.5
C 2	5-ring HIS 41	H-pi	4.05	−1.1
Cu(II) complex				
O 23	OD1 ASN 142	H-donor	2.81 (1.50)	−18.6
O 19	N GLY 143	H-acceptor	3.48 (2.57)	−0.6
O 21	N GLU 166	H-acceptor	3.25 (2.25)	−1.0

*The lengths of H-bonds are in brackets.

Table 5
The Docking interaction data calculations of ligand and Cu(II) complex with the active sites of the receptor of Proteus vulgaris (gram +ve bacteria) (PDB ID: 5i39).

	Receptor	Interaction	Distance(Å)*	E (kcal/mol)
L				
N 14	O THR 436	H-donor	2.99 (2.04)	−5.1
O 16	N THR 436	H-acceptor	3.50 (2.52)	−1.0
C 10	SE MSE 411	H-donor	3.73 (2.75)	−0.7
6-ring	N GLY 439	pi-H	3.98	−0.8
Cu(II) complex				
O 23	OE2 GLU 140 (A)	H-donor	2.64 (1.74)	−20.3
N 14	OE2 GLU 140 (A)	ionic	3.36	−2.5
O 23	OE2 GLU 140 (A)	ionic	2.64	−7.4

*The lengths of H-bonds are in brackets.

ve bacteria: E. coli (gram –ve bacteria) (PDB ID: 1fj4) are found to be −3.8 and −41.0 kcal/mol for the ligand and the Cu(II) complex; respectively, Table 6. The more negative the binding energy the stronger interaction. So, the interaction are in the order of Cu(II) complex > L.

3.3.4. Docking on the receptor of human DNA (PDB ID:1BNA)

The binding free energy of the ligand and the metal complex with the active sites of the receptor of human DNA (PDB ID:1BNA) are found to be −5.5 and −30.2 kcal/mol for the ligand and the Cu(II) complex; respectively, Table 7. The more negative the binding energy the stronger interaction. So, the interaction are in the order of Cu(II) complex > L.

The 2D and 3D plot of the interaction between L and Cu(II) complex with the active site of the receptor of human DNA (PDB ID:1BNA) are shown in Figs. 12 and 13.

3.4. ADMET prediction

In silico ADMET analysis is a quick approach to find if a compound has acceptable pharmacokinetics and pharmacodynamics properties. The toxicity risks and bioavailability of the ligand compound was predicted based on ADMET profile (Table 8).

Results showed a good human intestinal absorption probability, a favorable general distribution at the plasma level, except for the blood-brain barrier (BBB) it has a poor distribution and optimal toxicity except for drug-induced liver damage. The prediction

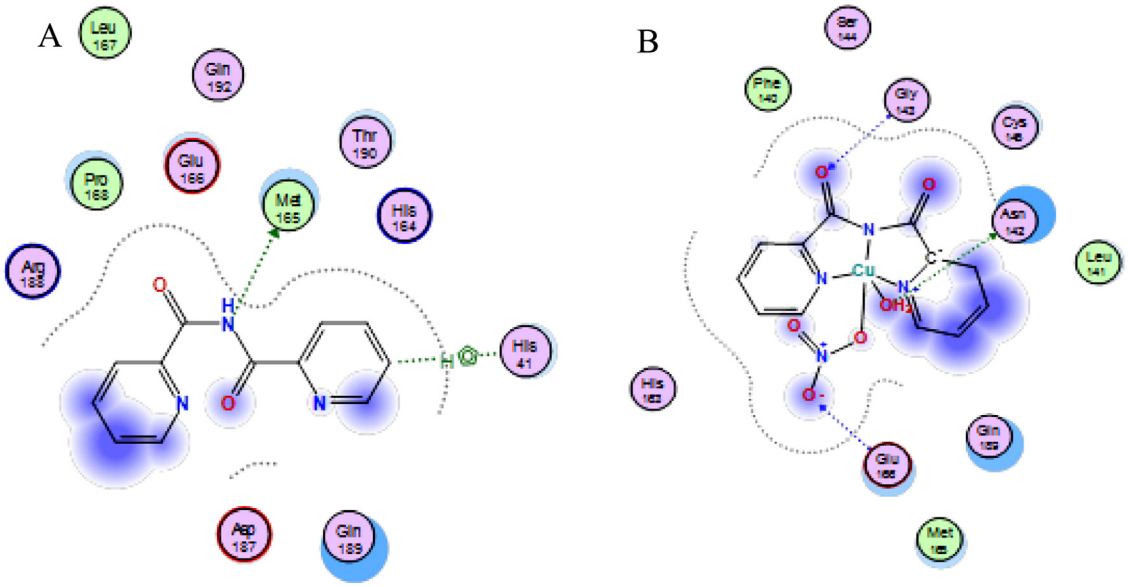

Fig. 6. 2D plot of the interaction between L (A) and Cu(II) complex (B) with the active site of the receptor of viral protein (PDB ID: 6lu7). Hydrophobic interactions with amino acid residues are shown with dotted curves.

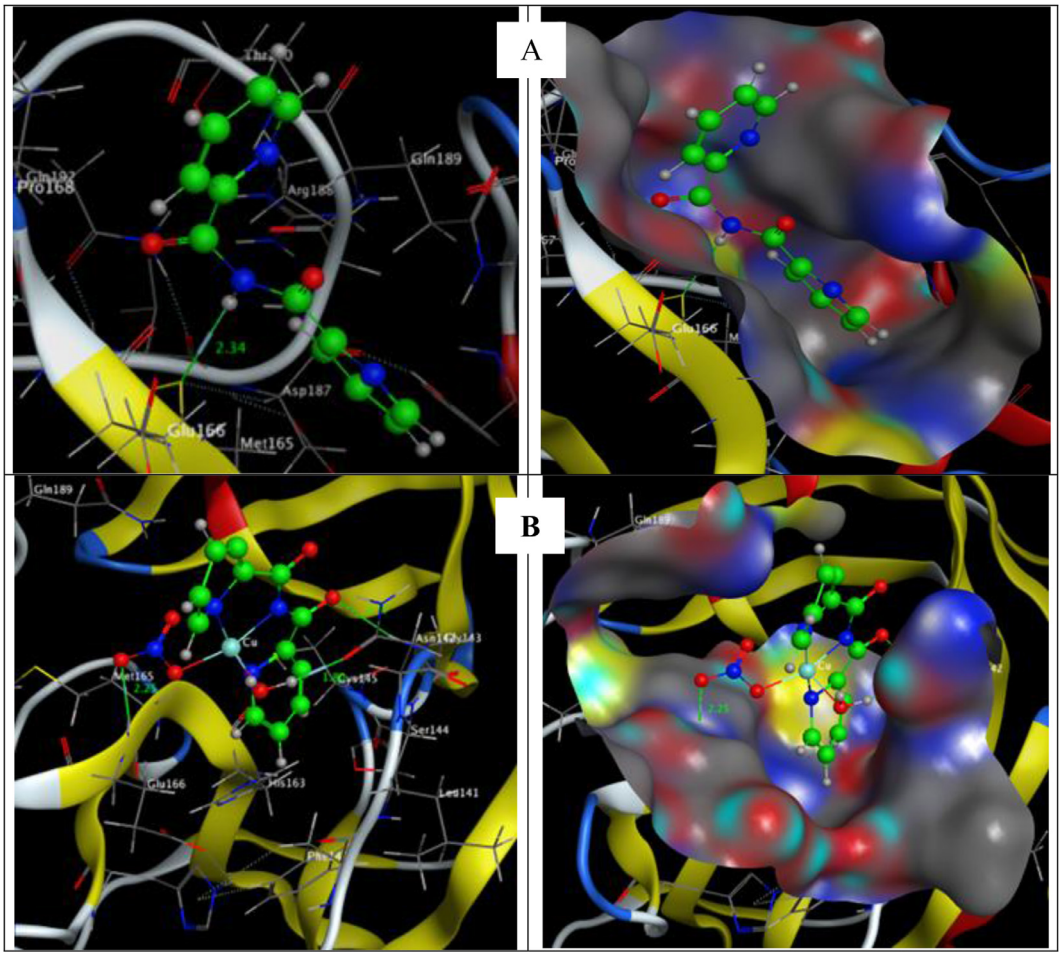

Fig. 7. Molecular docking simulation studies of the interaction between L (A) and Cu(II) complex (B) with the active site of the receptor of viral protein (PDB ID: 6lu7). The docked conformation of the compound is shown in ball and stick representation.

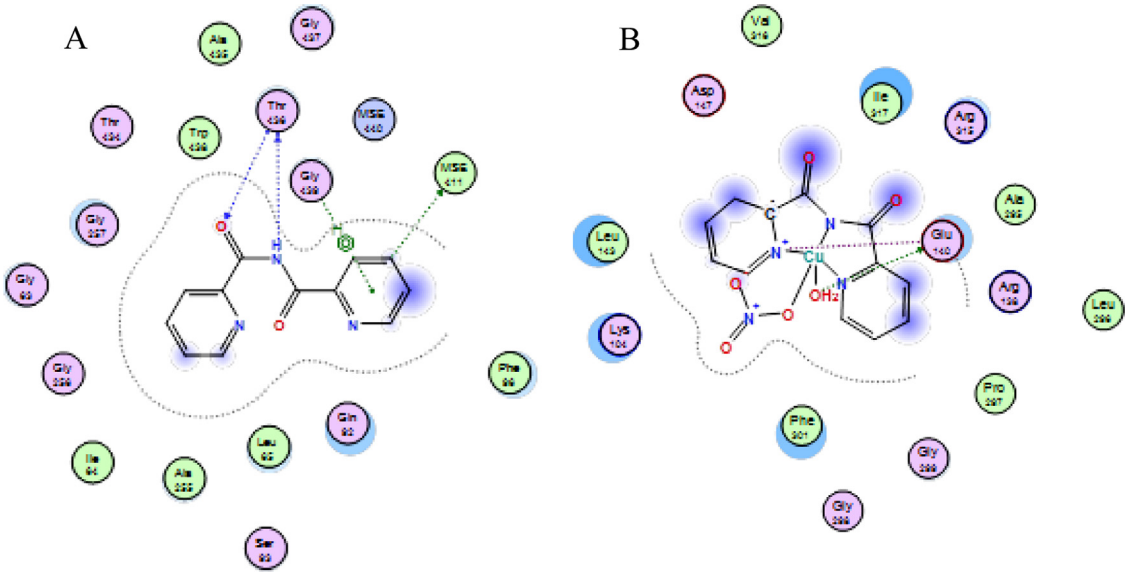

Fig. 8. 2D plot of the interaction between L (A) and Cu(II) complex (B) with the active site of the receptor of Proteus vulgaris (PDB ID: 5i39). Hydrophobic interactions with amino acid residues are shown with dotted curves.

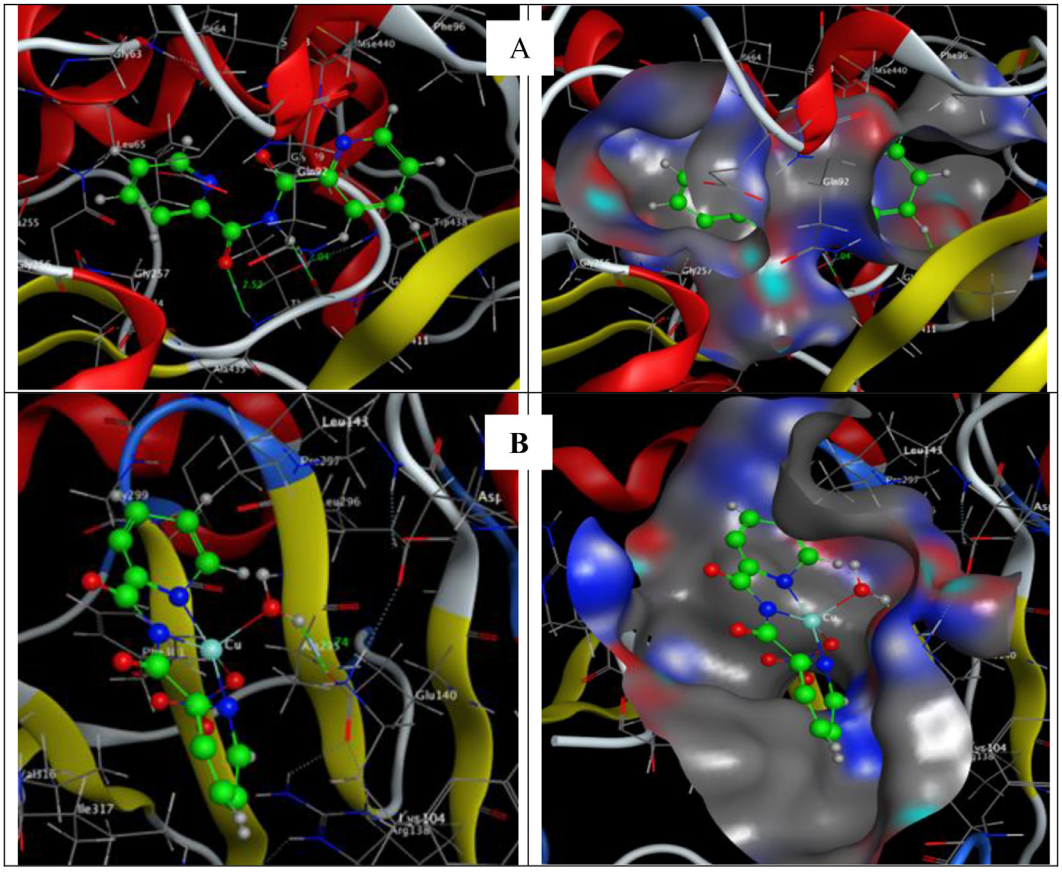

Fig. 9. Molecular docking simulation studies of the interaction between L (A) and Cu(II) complex (B) with the active site of the receptor of Proteus vulgaris (PDB ID: 5i39). The docked conformation of the compound is shown in ball and stick representation.

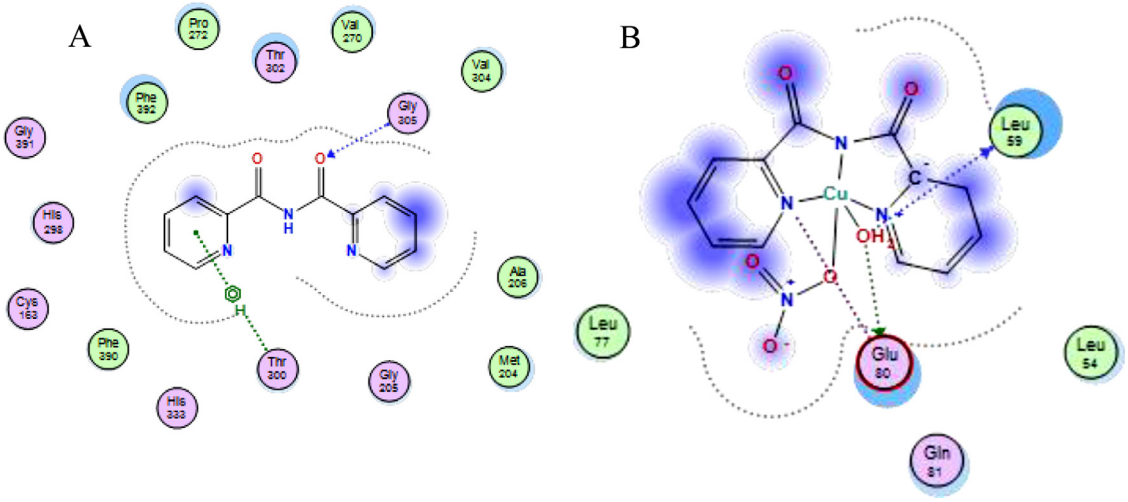

Fig. 10. 2D plot of the interaction between L (A) and Cu(II) complex (B) with the active site of the receptor of Escherichia coli (PDB ID: 1fj4). Hydrophobic interactions with amino acid residues are shown with dotted curves.

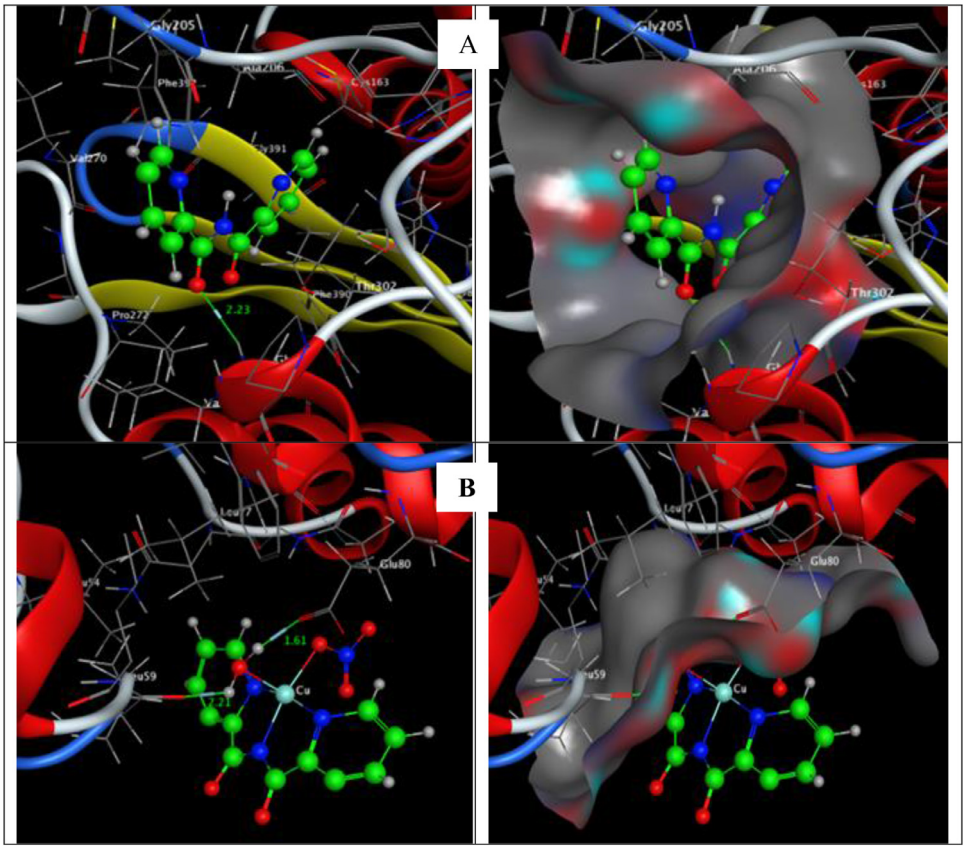

Fig. 11. Molecular docking simulation studies of the interaction between L (A) and Cu(II) complex with the active site of the receptor of Escherichia coli (PDB ID: 1fj4). The docked conformation of the compound is shown in ball and stick representation.

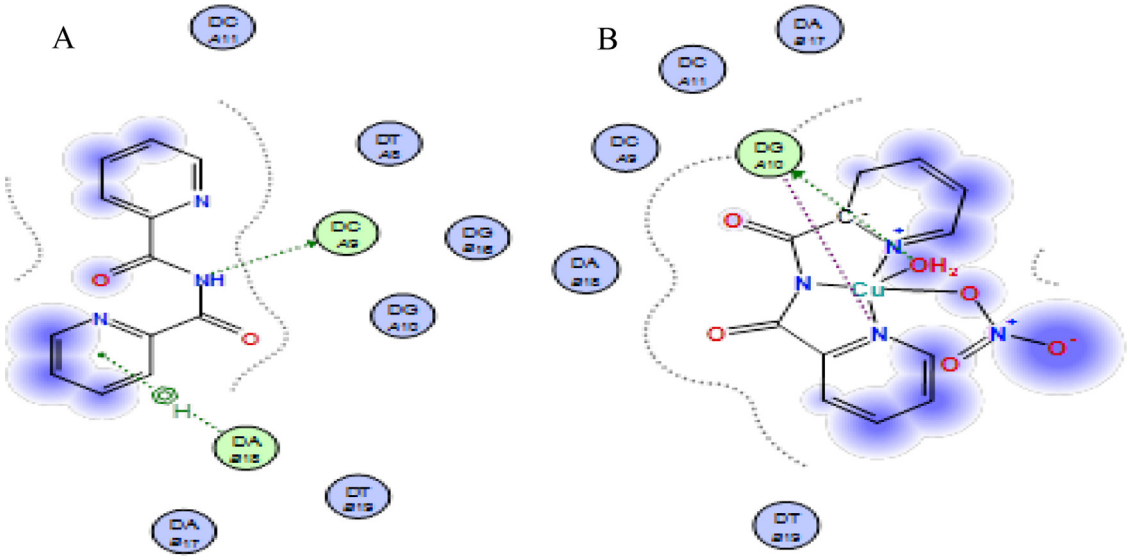

Fig. 12. 2D plot of the interaction between L (A) and Cu(II) complex (B) with the active site of the receptor of human DNA (PDB ID:1BNA). Hydrophobic interactions with amino acid residues are shown with dotted curves.

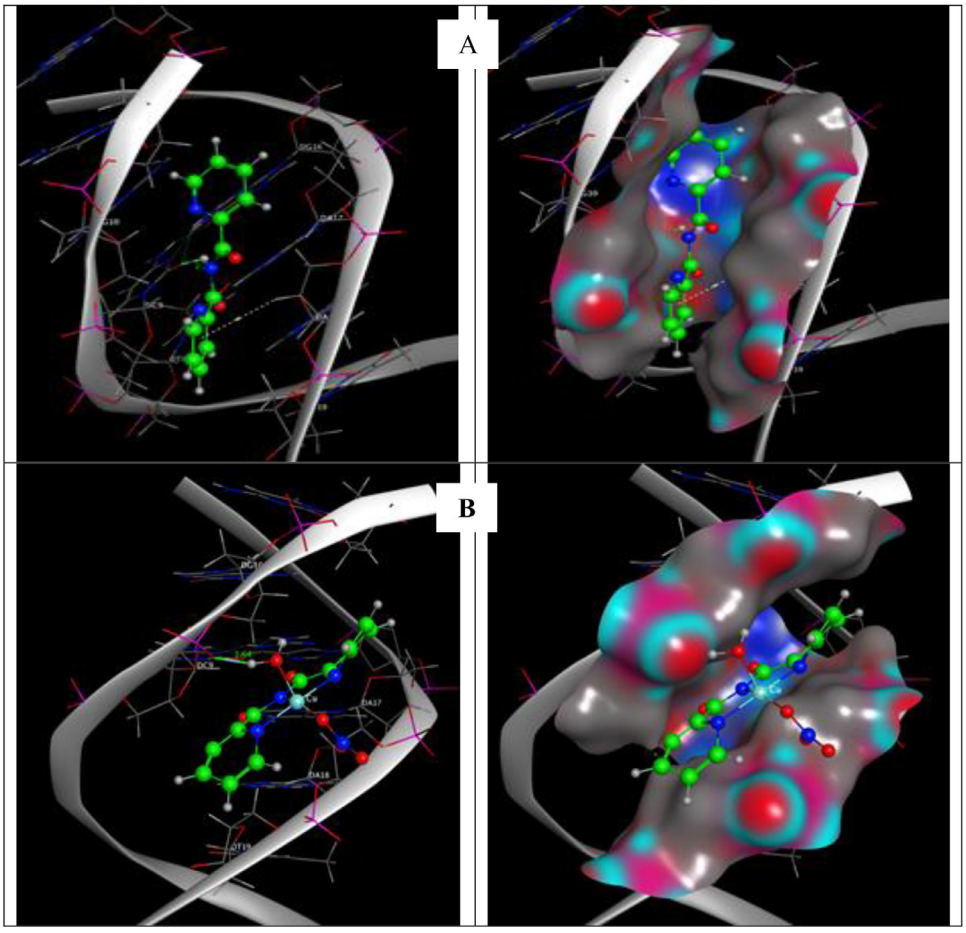

Fig. 13. Molecular docking simulation studies of the interaction between L (A) and Cu(II) complex with the active site of the receptor of human DNA (PDB ID:1BNA). The docked conformation of the compound is shown in ball and stick representation.

Table 6
The Docking interaction data calculations of ligand and Cu(II) complex with the active sites of the receptor of Escherichia coli (gram –ve bacteria) (PDB ID: 1fj4).

	Receptor	Interaction	Distance(Å)*	E (kcal/mol)
L				
O 17	N GLY 305	H-acceptor	3.11 (2.23)	−1.7
6-ring	OG1 THR 300	pi-H	4.43	−1.2
6-ring	CG2 THR 300	pi-H	4.12	−0.9
Cu(II) complex				
O 23	OE1 GLU 80	H-donor	2.60 (1.61)	−24.0
O 23	O LEU 59	H-donor	3.00 (2.21)	−4.7
O 23	OE1 GLU 80	ionic	2.60	−7.8
N 16	OE1 GLU 80	ionic	3.22	−3.1
N 16	OE2 GLU 80	ionic	3.65	−1.4

*The lengths of H-bonds are in brackets.
The 2D and 3D plot of the interaction between L and Cu(II) complex with the active site of the receptor of E. coli (gram –ve bacteria) (PDB ID: 1fj4) are shown in Figs. 10 and 11.

Table 7
The Docking interaction data calculations of ligand and Cu(II) complex with the active sites of the receptor of human DNA (PDB ID:1BNA).

	Receptor	Interaction	Distance(Å)*	E (kcal/mol)
L				
N 14	O2 DC 9 (A)	H-donor	3.14 (2.23)	−4.9
6-ring	C4′ DA 18 (B)	pi-H	4.51	−0.6
Cu(II) complex				
O 23	OP1 DG 10 (A)	H-donor	2.64 (1.64)	−20.7
N 16	OP1 DG 10 (A)	Ionic	3.45	−2.1
O 23	OP1 DG 10 (A)	Ionic	2.64	−7.4

*The lengths of H-bonds are in brackets.

results showed also that no carcinogenic effects and no AMES toxicity were found.

4. Conclusion

Crystal structure analysis the complex [Cu(dipicolinoylamide)(NO_3)(H_2O)] shows it crystallizes in space group $P2_1/n$ and the copper center has a distorted octahedral geometry. DFT calculations show good agreement between theoretical and X-ray data.

Our complex of Cu (II) has been investigated as an inhibitor for COVID-19 by a molecular docking study. The binding free energy of the ligand and the metal complex with the active sites of the receptor of COVID-19 main protease viral protein (PDB ID: 6lu7), are found to be −5.6 and −20.2 kcal/mol for the ligand and the Cu(II) complex; respectively. This suggests that this complex may merit further study in the context of possible therapeutic agents for COVID-19.

In addition, the result of molecular docking studies show the binding free energy of the Cu(II) complex with the active sites of the receptor of gram -ve bacteria: E. coli (gram –ve bacteria) (PDB ID: 1fj4), of gram +ve bacteria: Proteus vulgaris (PDB ID: 5i39) and revealed that for the studied complex, the more negative the binding energy the stronger interaction. So, the interaction are in the order of Cu(II) complex > L. Furthermore, the molecular docking studies indicated that the investigated Cu(II) complex has a good binding affinity with human DNA and reveals that the title molecule forms a stable complex with DNA with the binding affinity value −41.0 kcal/mol and shows that it can increase the stability of DNA. Indeed, ADMET outcomes of the predicted compound are depicted good pharmacokinetic properties with the good absorption, acceptable metabolism transformation, and are found to be neither toxic, which can be granted as reliable inhibitors for SARS-CoV-2.

Table 8
Calculated ADMET properties.

Property	Value
Absorption	
Caco-2 Permeability	−4.556
MDCK Permeability	2.6e-05
Pgp-inhibitor	0.001
Pgp-substrate	0.013
HIA	0.012
$F_{20\%}$	0.02
$F_{30\%}$	0.012
Distribution	
PPB	56.80%
VD	1.07
BBB Penetration	0.918
Fu	45.31%
Metabolism	
CYP1A2 inhibitor	0.187
CYP1A2 substrate	0.054
CYP2C19 inhibitor	0.047
CYP2C19 substrate	0.062
CYP2C9 inhibitor	0.028
CYP2C9 substrate	0.851
CYP2D6 inhibitor	0.002
CYP2D6 substrate	0.162
CYP3A4 inhibitor	0.004
CYP3A4 substrate	0.14
Excretion	
CL	0.629
$T_{1/2}$	0.668
Toxicity	
hERG Blockers	0.127
H-HT	0.071
DILI	0.978
AMES Toxicity	0.052
Rat Oral Acute Toxicity	0.308
FDAMDD	0.322
Skin Sensitization	0.206
Carcinogen city	0.031
Eye corrosion	0.003
Eye irritation	0.7
Respiratory Toxicity	0.412
Bioconcentration Factors	0.312
IGC_{50}	1.902
$LC_{50}FM$	2.6
$LC_{50}DM$	3.896
Tox21 pathway	
NR-AR	0.009
NR-AR-LBD	0.025
NR-AhR	0.022
NR-Aromatase	0.053
NR-ER	0.125
NR-ER-LBD	0.005
NR-PPARgamma	0.757
SR-ARE	0.247
SR-ATAD5	0.618
SR-HSE	0.043
SR-MMP	0.036
SR-p53	0.843

Declaration of Competing Interest

The authors of this manuscript report that there are no conflicts of interest relevant to this research work.

Supplementary materials

Supplementary material associated with this article can be found, in the online version, at doi:10.1016/j.molstruc.2021.131348.

CRediT authorship contribution statement

Laila H. Abdel-Rahman: Project administration, Investigation, Supervision, Writing – original draft. **Maram T. Basha:** Formal

analysis, Investigation, Methodology, Writing – original draft. **Badriah Saad Al-Farhan:** Formal analysis, Investigation, Methodology, Writing – original draft. **Mohamed R. Shehata:** Data curation, Software, Validation, Visualization. **Shaaban K. Mohamed:** Project administration, Investigation, Supervision, Writing – original draft. **Youssef Ramli:** Data curation, Software, Validation, Visualization.

References

[1] R. Lu, W. Wang, X. Li, Clinical observation on the treatment of 63 suspected cases of novel coronavirus pneumonia with traditional Chinese medicine Lianhua Qingwen, J. Tradit. Chin. Med. 61 (2020) 655–659.

[2] L. Runfeng, H. Yunlong, H. Jicheng, P. Weiqi, M. Qinhai, S. Yongxia, L. Chufang, Z. Jin, J. Zhenhua, J. Haiming, Z. Kui, H. Shuxiang, D. Jun, L. Xiaobo, H. Xiaotao, W. Lin, Z. Nanshan, Y. Zifeng, Lianhuaqingwen exerts anti-viral and anti-inflammatory activity against novel coronavirus (SARS-CoV-2), Pharmacol. Res. 156 (2020) 104761, doi:10.1016/j.phrs.2020.104761.

[3] Y.W. David Lee, Y. Qing Li, J. Liu, T. Efferth, Traditional Chinese herbal medicine at the forefront battle against COVID-19: clinical experience and scientific basis, Phytomedicine 80 (2021) 153337, doi:10.1016/j.phymed.2020.153337.

[4] M.M.Can O.Sogut, R. Guven, H.Ergenc O.Kaplan, T.B. Umit, M.Kaya O.Demir, T. Akdemir, S. Cakmak, Safety and efficacy of hydroxychloroquine in 152 outpatients with confirmed COVID-19: A pilot observational study, Am. J. Emergency Med. 40 (2021) 41–46, doi:10.1016/j.ajem.2020.12.014.

[5] C.D. Russell, J.E. Millar, J.K. Baillie, Clinical evidence does not support corticosteroid treatment for 2019-nCoV lung injury, Lancet 395 (2020) 473–475, doi:10.1016/S0140-6736(20)30317-2.

[6] F. Cantini, L. Niccoli, D. Matarrese, E. Nicastri, P. Stobbione, D. Goletti, Baricitinib therapy in COVID-19: A pilot study on safety and clinical impact, J. Infect. 81 (2020) 318–356, doi:10.1016/j.jinf.2020.04.017.

[7] L. Pasin, G. Cavalli, P. Navalesi, N. Sella, G. Landoni, G. Yavorovskiy, V. Valery, A. Zangrillo, L. Dagna, G. Monti, Anakinra for patients with COVID-19: a meta-analysis of non-randomized cohort studies, Eur. J. Intern. Med. 86 (2020) 34–40, doi:10.1016/j.ejim.2021.01.016.

[8] G. Cavalli, G. De Luca, C. Campochiaro, E. Della Torre, M. Roipa, D. Canetti, et al., Interleukin-1 blockade with high-dose anakinra in patients with COVID-19, acute respiratory distress syndrome, and hyperinflammation: a retrospective cohort study, Lancet Rheumatol. 2 (2020) 325–331, doi:10.1016/S2665-9913(20)30127-2.

[9] B. Cao, Y. Wang, D. Wen, W. Liu, J. Wang, G. Fan, et al., A trial of Lopinavir-Ritonavir in adults hospitalized with severe Covid-19, N. Engl. J. Med. 382 (2020) 1787–1799, doi:10.1056/NEJMoa2001282.

[10] J.M. Sanders, M.L. Monogue, T.Z. Jodlowski, et al., Pharmacologic treatments for coronavirus disease 2019 (COVID-19) A Review, JAMA 323 (2020) 1824–1836, doi:10.1001/jama.2020.6019.

[11] P. Luo, Y. Liu, L. Qiu, X. Liu, D. Liu, J. Li, Tocilizumab treatment in COVID-19: a single center experience, J. Med. Virol. (2020), doi:10.1002/jmv.25801.

[12] M. Colaneri, L. Bogliolo, P. Valsecchi, P. Sacchi, V. Zuccaro, F. Brandolino, et al., Tocilizumab for treatment of severe COVID-19 patients: preliminary results from SMAtteo COvid19 REgistry (SMACORE), Microorganisms 8 (2020) 695, doi:10.3390/microorganisms8050695.

[13] L. Quartuccio, A. Sonaglia, D. McGonagle, M. Fabris, M. Peghin, D. Pecori, et al., Efficacy and safety of tocilizumab in severe COVID-19 patients: a single-centre retrospective cohort study, J. Clin. Virol. 129 (2020) 104444.

[14] C. Campochiaro, E. Della-Torre, G. Cavalli, G. De Luca, M. Ripa, N. Boffini, et al., Efficacy and safety of tocilizumab in severe COVID-19 patients: a single-centre retrospective cohort study, Eur. J. Intern. Med. 76 (2020) 43–49, doi:10.1016/j.ejim.2020.05.021.

[15] M. Parsey, An open letter from Merdad Parsey, Chief Medical Officer, Gilead Sciences, 2020. https://stories.gilead.com/articles/open-letter-from-merdad-par sey, (Accessed 22 October 2020).

[16] E.I. Lerner, S.J. Lippard, 2,4,6-Tris(2-pyrimidyl)- and 2,4,6-tris(2-pyridyl)-1,3,5-triazines hydrolyze in the presence of copper(II) to form a novel bis(aryl)carboximidato chelate complex, J. Am. Chem. Soc. 98 (1976) 5397, doi:10.1021/ja00433a061.

[17] E.I. Lerner, S.J. Lippard, Heavy-metal complexes of 2,4,6-tris(2-pyrimidyl)-1,3,5-triazine. Structure of a dilead derivative, Inorg. Chem. 16 (1977) 1546, doi:10.1021/ic50172a059.

[18] P. Paul, B. Tyagi, M.M. Bhadbhade, E. Suresh, Predominance of electron-withdrawing effect over angular strain in the metal-promoted hydrolysis of 2,4,6-tris(2-pyridyl)-1,3,5-triazine, J. Chem. Soc. Dalton Trans. (1997) 2273, doi:10.1039/A608433H.

[19] P. Paul, B. Tyagi, A.K. Bilakhiya, M.M. Bhadbade, G. Ramachandaiah, Synthesis and characterization of rhodium complexes containing 2,4,6-Tris(2-pyridyl)-1,3,5-triazine and its metal-promoted hydrolytic products: potential uses of the new complexes in electrocatalytic reduction of carbon dioxide, Inorg. Chem. 37 (1998) 5733, doi:10.1021/ic9709739.

[20] BrukerProgram Name(S), Bruker AXS Inc., Madison, Wisconsin, 2012.

[21] BrukerProgram Name, Bruker AXS Inc., Madison, Wisconsin, USA, 2001.

[22] G.M. Sheldrick, SHELXT - Integrated space-group and crystal-structure determination, Acta Cryst. A71 (2015) 3–8, doi:10.1107/S2053273314026370.

[23] G.M. Sheldrick, SHELX: applications to macromolecules, Kluwer Academic Publishers, Dordrecht, 1998, pp. 401–411, doi:10.1007/978-94-015-9093-8_35.

[24] G.M. Sheldrick, Report on a project on three-dimensional imaging of the biological cell by single-particle X-ray diffraction, Acta Crystallographica Section A 64 (2008) 112–122, doi:10.1107/S010876730705550X.

[25] M.A. Robb, J.R. Cheeseman, G. Scalmani, B. Mennucci, V. Barone, G.A. Petersson, H. Nakatsuji, M. Caricato, H.P. Hratchian, X. Li, A.F. Izmaylov, J. Bloino, J.L. Sonnenberg, G. Zheng, M. Hada, M. Ehara, K. Toyota, J. Hasegawa, R. Fukuda, M. Ishida, T. Nakajima, Y. Honda, O. Kitao, T. Vreven, J.A. Montgomery, J.E. Peralta, H. Nakai, F. Ogliaro, M. Bearpark, J.J. Heyd, K.N. Kudin, V.N. Staroverov, R. Kobayashi, E. Brothers, J. Normand, K. Raghavachari, A. Rendell, S.S. Iyengar, J. Tomasi, J.C. Burant, M. Cossi, N. Rega, J.M. Millam, M. Klene, J.E. Knox, V. Bakken, C. Adamo, J. Jaramillo, R. Gomperts, J.B. Cross, R.E. Stratmann, O. Yazyev, R. Cammi, C. Pomelli, J.W. Ochterski, A.J. Austin, R.L. Martin, K. Morokuma, V.G. Zakrzewski, P. Salvador, J.J. Dannenberg, G.A. Voth, S. Dapprich, A.D. Daniels, O. Farkas, J.V. Ortiz, J. Cioslowski, J.B. Foresman, D.J. Fox, Gaussian 09, Gaussian Inc., Wallingford CT, 2009.

[26] H. Moustafa, G.G. Mohamed, S. Elramly, Spectroscopic studies, Density Functional Theory calculations, and non-linear optical properties of binuclear Fe(III), Co(II), Ni(II), Cu(II), and Zn(II) complexes of OONN Schiff base ligand, J. Chin. Chem. Soc. 67 (2020) 1783–1793, doi:10.1002/jccs.202000024.

[27] Molecular Operating Environment (MOE), 2019. 01; Chemical Computing Group ULC, 1010 Sherbrooke St. West, Suite #910, Montreal, QC, Canada, H3A 2R7, 2019.

[28] Z. Jin, X. Du, Y. Xu, Y. Deng, M. Liu, Y. Zhao, H. Yang, Structure of M^{pro} from SARS-CoV-2 and discovery of its inhibitors, Nature 582 (2020) 289–293, doi:10.1038/s41586-020-2223-y.

[29] A.C. Price, K.H. Choi, R.J. Heath, Z. Li, S.W. White, C.O. Rock, Inhibition of b-Ketoacyl-Acyl Carrier Protein Synthases by Thiolactomycin and Cerulenin, J. Biol. Chem. 276 (2001) 6551–6559, doi:10.1074/jbc.M007101200.

[30] S.K. Srivastava, K. Rajasree, B. Gopal, Conformational basis for substrate recognition and regulation of catalytic activity in Staphylococcus aureus nucleoside di-phosphate kinase, Biochimica et Biophysica Acta (BBA)-Proteins Proteomics 1814 (2011) 1349–1357, doi:10.1016/j.bbapap.2011.06.008.

[31] Y. Ju, S. Tong, Y. Gao, W. Zhao, Q. Liu, Q. Gu, H. Zhou, Crystal structure of a membrane-bound l-amino acid deaminase from Proteus vulgaris, J. Struct. Biol. 195 (2016) 306–315, doi:10.1016/j.jsb.2016.07.008.

[32] H. Laila Abdel-Rahman, R. Ramadan, Synthesis and characterization of some new mono- and binuclear copper(II) ternary complexes; X-ray crystal structure of copper(II)- *N* -(acetyl)phenylglycinateimidazole ternary complex, J. Coord. Chem. 60 (2007) 1891–1901, doi:10.1080/00958970701209864.

[33] H. Laila Abdel-Rahman, Complexes of zinc(II) and cadmium(II) with N-phthaloylglycinate, imidazole, 5-amino tetrazole and 2,4,6- *tris* (2-pyridyl)-1,3,5-triazine. X-ray crystal structure of $[Cd(imi)_3(N\text{-phthgly})_2]2H_2O$, J. Coord. Chem. 60 (2007) 865–875, doi:10.1080/00958970600961664.

[34] Laila H. Abdel-Rahman, G. Bocelli, Synthesis and spectroscopic properties of copper(II)-N- phthaloylglycinate derivatives of imidazole, methylimidazole, 1,10-phenanthroline and 2,2′,2″-terpyridine. Crystal structure of $[Cu(OH_2)_2(phen)(N\text{-phthgly})]\ (NO_3)\ H_2O$ and $[Cu(terpy)(N\text{-phthgly})_2]\cdot H_2O$, J. Coord. Chem. 59 (2006) 1385–1394, doi:10.1080/00958970600556928.